Investigation of very low mass binaries using *VLT*/NaCo

Subhajeet Karmakar [1,2]† A. S. Rajpurohit,[2] and D. Homeier[3,4]

[1] Monterey Institute for Research in Astronomy (MIRA), 200 Eighth Street, Marina, California 93933, USA
[2] Astronomy & Astrophysics Division, Physical Research Laboratory, Navrangapura, Ahmedabad 380009, India
[3] Aperio Software Ltd., Insight House, Riverside Business Park, Stoney Common Road, Stansted, Essex, CM24 8PL, UK
[4] Förderkreis Planetarium Göttingen, 37085 Göttingen, Germany

Abstract

Context: Most stars in the galactic stellar population are low-mass stars. Very low mass (VLM) stars are a subset of the low-mass stars typically defined in terms of the stellar masses ranging from 0.6 $M_\odot$ to the hydrogen-burning limit of about 0.075 $M_\odot$.
Aim: The observational studies of VLM binaries can provide effective diagnostics for testing the VLM formation scenarios. The small size of VLMs makes them suitable candidates to detect planets around them in the habitable zone.
Methods: In this work, using the high-resolution near-infrared adaptive optics imaging from the NaCo instrument installed on the Very Large Telescope, we report the discovery of a new binary companion to the M-dwarf LP 1033-31 and also confirm the binarity of LP 877-72. We have characterized both stellar systems and estimated the properties of their individual components.
Results and Conclusions: We have found that LP 1033-31 AB with the spectral type of M4.5+M4.5 has a projected separation of 6.7±1.3 AU. On the other hand, with the spectral type of M1+M4, the projected separation of LP 877-72 AB is estimated to be 45.8±0.3 AU. We further investigated the masses, surface gravity, radii, and effective temperature of the detected components. The orbital period of LP 1033-31 and LP 877-72 systems are estimated to be ~28 and ~349 yr, respectively. Our analysis suggests that there is a possibility of finding up to 'two' exoplanets around LP 877-72 B. In contrast, the maximum probability of hosting exoplanets around LP 877-72 A, LP 1033-31 A, and LP 1033-31 B are estimated to be only ~50%.

1 Introduction

Low mass stars with partially or fully convective envelops show a high level of magnetic activities (see Pandey & Karmakar, 2015; Patel et al., 2016; Savanov et al., 2016, 2019; Karmakar, 2019, 2021; Karmakar et al., 2016, 2017, 2022, 2023). Recent studies have shown the magnetic activities also increase for the later spectral types (e.g., Savanov et al., 2018; Karmakar & Pandey, 2018; Karmakar et al., 2019). Typically, the stars with a mass range of 0.075–0.6 $M_\odot$ are called very low mass stars (VLMs). The VLMs are intrinsically faint due to their small size and low temperature. However, the latest studies with several ground-based surveys, including SDSS (York et al., 2000) and 2MASS (Skrutskie et al., 2006), and space-based surveys including WISE (Wright et al., 2010) have made discoveries of the VLM stars. The observational studies of the VLM stars provide effective diagnostics for testing the VLM star formation scenarios. The VLM binaries (= VLM + VLM) are of particular interest because the formation mechanisms leave their own traces on the statistical properties of the binaries, such as frequency, orbital separation, and mass-ratio distribution (e.g. Bate, 2009). Moreover, the VLM binaries also provide the model-independent way to determine the physical properties, including masses and radii (see Delfosse et al., 2000; Dupuy & Liu, 2017; Winters et al., 2019).

In recent years the adaptive optics (AO) imaging and radial velocity (RV) survey have made a valuable contribution

to the discovery of the VLM binaries. Due to their small size, VLM stars also are suitable candidates for detecting exoplanets around them in the habitable zone. Recently, a few extensive exoplanet surveys such as the M2K program (Apps et al., 2010), CARMENES search for exoplanets (Reiners et al., 2018), and MEarth project (Dittmann et al., 2016) investigated exoplanets around a sizeable number of M-dwarfs. The presence of the companion to the primary VLM star is also significant as they influence planet formation. However, due to limited detection of exoplanetary systems in the binary or multiple systems, particularly on VLM stellar systems, the study of stellar multiplicity's effect on planet formation is still statistically insignificant. In the solar neighborhood, planets in multiple-star systems are found to occur 4.5±3.2, 2.6±1.0, and 1.7±0.5 times less frequently than the single-star systems when a stellar companion is present at a distance of 10, 100, and 1000 AU, respectively. Therefore, further observations of the VLM binaries are essential.

Investigation of VLM stars with high spatial resolution imaging enabled us to discover new companions to the previously known 'single' stellar system. This investigation is essential to have a better understanding of the stellar system and have a precise estimation of the binary separation for VLM stars. Significant progress has been made in this direction in the last few decades. Summarizing the results of the high spatial resolution imaging surveys of VLM stars published in dozens of articles between 1991 and 2005, Phan-Bao et al. (2005) found the binary frequency in the separation range 1–15 AU was about 15%, whereas for wide binary systems (semi-major axis >15 AU), the binary frequency was very low, <1%. Using statistical investigation utiliz-

ing a Bayesian algorithm Allen et al. (2012) found that only 2.3% of VLM objects have a companion in the 40–1000 AU range. While the last two sources cannot be directly compared due to different input sample sizes, the older studies might have underestimated the binary fraction or were still incomplete. Further, Baron et al. (2015) discovered 14 VLM binary systems with separations of 250–7500 AU. Gálvez-Ortiz et al. (2017) identified 36 low-mass and VLM candidates to binary/multiple systems with separations between 200 and 92 000 AU. These differences can be due to a continuous formation mass-dependent trend or differences in the VLM objects' formation mechanism. Further high-resolution study of VLM binaries provides valuable constraints for the formation mechanism of VLM binaries.

2   The Objects

In this paper, we discussed near-infrared (NIR) detection of VLM companions to two M-dwarfs LP 1033-31 and LP 877-72 using direct imaging. Both the objects are far from the galactic plane, and they were first detected as part of HPM surveys (Giclas et al., 1978; Luyten, 1995). Since a star's proper motion (PM) is inversely proportional to its distance from the observer, a high proper motion (HPM) is a strong selection criterion for proximity. Further observations of these objects were carried out as part of several high proper-motion surveys (Wroblewski & Torres, 1995; Pokorny et al., 2003; Salim & Gould, 2003; Reylé & Robin, 2004; Schneider et al., 2016; Kirkpatrick et al., 2016). The latest estimated values for proper motion of the systems are 0″.299 and 0″.305 per year for LP 1033-31 and LP 877-72, respectively (Muirhead et al., 2018; Stassun et al., 2019). Both of these objects were also studied as a part of the bright M-dwarfs (Lépine & Gaidos, 2011; Frith et al., 2013), as well as the solar-neighborhoods (Finch et al., 2014; Winters et al., 2015). We discovered LP 1033-31 is a VLM binary system rather than a 'single' object, as known previously. Moreover, we also confirmed the binarity of LP 877-72 after the *Gaia* detection of the companion (Gaia Collaboration et al., 2018). Please find the paper Karmakar et al. (2020) for the detailed investigation.

3   The observatory and the AO system

The observations were taken from the Very Large Telescope (VLT) of the European Southern Observatory (ESO, Chile). The Nasmyth Adaptive Optics System (NAOS; Rousset et al., 1998, 2000) delivers diffraction-limited images to the Coudé Near Infrared Camera (CONICA; Lenzen et al., 1998; Hartung et al., 2000). The combined system is popularly known as NaCo. NAOS is installed at one of the Nasmyth foci, and it corrects an f/15 beam for atmospheric turbulence and hands-on again an f/15 beam providing CONICA with diffraction-limited images. The wavefront sensing path consists of a field selector (Spanoudakis et al., 2000) and two wavefront sensors (WFS). They are located between the dichroic mirror and the WFS input focus. Please see Hartung et al. (2003) and references therein.

4   Observations

Using the VLT/NaCo instrument, two M-dwarfs LP 1033-31 and LP 877-72 were observed under program ID 091.C-0501(B). On 2013 July 02, a total of 20 and 30 frames were observed in each of the NIR JHK_s photometric bands for LP 1033-31 and LP 877-72, respectively. The exposure time for individual frames was 30 s. Each image was jittered using a jitter box of 5″ to allow an efficient reduction of the sky background. Due to the fact that no bright adaptive optics (AO) source was available nearby, N90C10 dichroic was used, where 90% of the light was utilized for AO and only 10% for the science camera. S13 camera was used with a field of view of 14″ × 14″ and a pixel scale of 13.2 mas per pixel. The airmass of LP 1033-31 and LP 877-72 were in the range of 1.049 – 1.051 and 1.002 – 1.010, respectively. The seeing condition for the day of observation was also very good (< 0.85″).

5   Data Analysis

In this research, we used the raw image mode data that were provided in ESO archive[*]. The data reduction was performed using the *Image Reduction and Analysis Facility* (IRAF[†]; Tody, 1986, 1993) software. In order to perform various operations, including source coordinate detection, position angle, and separation measurements, we have used python packages, including PHOTUTILS[‡] (Bradley et al., 2022), PYASTRONOMY[§] (Czesla et al., 2019), and ASTROPY[¶] (Astropy Collaboration et al., 2022). In order to perform the near-infrared (NIR) photometry in JHK_s photometric bands, we followed the standard procedures. Please see Karmakar et al. (2020) for more details about the reduction methods.

6   Brightness and Binary Separation

Fig. 1 shows the close-up view of the representative *J*-band images for the objects LP 1033-31 and LP 877-72. In the figure, the usual conventions were followed, i.e., north is up, and east is left. Both objects are clearly resolved as binary systems. In our analysis, the brighter component is considered primary. Fig. 1a indicates the LP 1033-31 system containing two components with the measured *J*-band magnitudes of 9.82±0.04 and 9.90±0.04. The components have almost equal brightness with a slightly higher flux of the South-East component (LP 1033-31 A) than the North-West component (LP 1033-31 B). For the LP 877-72 system, the *J*-band magnitudes are derived as 9.08±0.03 for the primary (LP 1033-31 A), and 10.77±0.04 (LP 877-72 B) for the secondary component. The binary separations for the LP 1033-31 and LP 877-72 systems have been estimated to be 402±1 and 1335±2 mas, respectively. Following Finch et al. (2014) and Bailer-Jones et al. (2018), in this work, we have adopted the distances for LP 1033-31 and LP 877-72 to be 16.57±3.27 and 33.77±0.17 pc, respectively. Therefore, the binary separation between the primary and secondary components of LP 1033-31 is computed as 6.7±1.3 AU. Similarly, the binary separation between LP 877-72 A and B is derived as 45.8±0.3 AU.

7   Absolute magnitude and Spectral Type

The absolute *J*-band magnitude for the primary and secondary components of LP 1033-31 are derived to be 8.7±0.4 and 8.8±0.4, respectively. On the other hand, for the primary
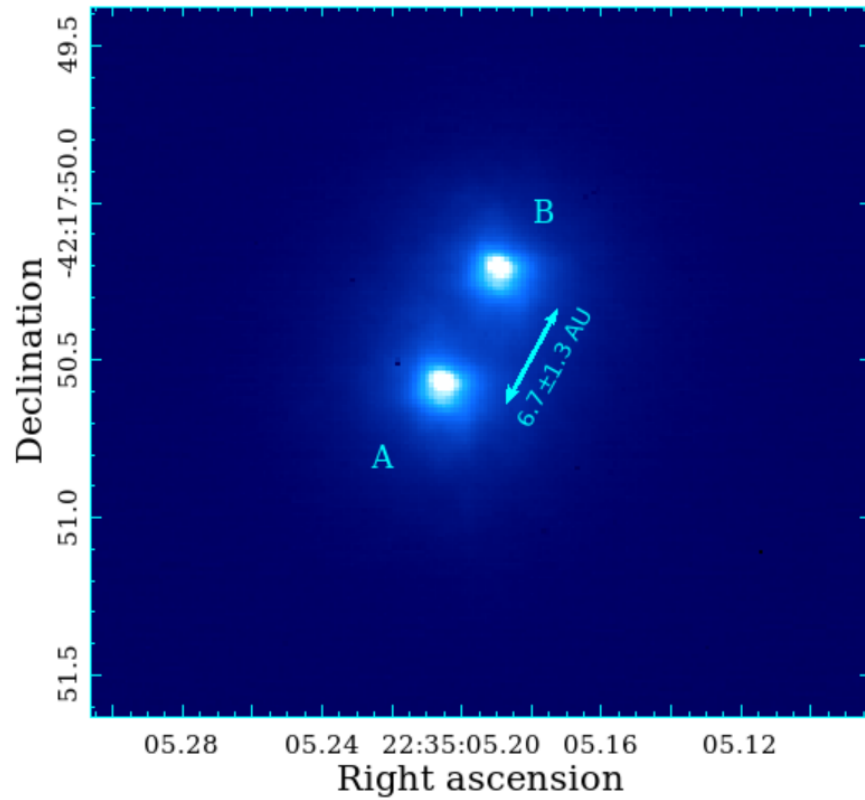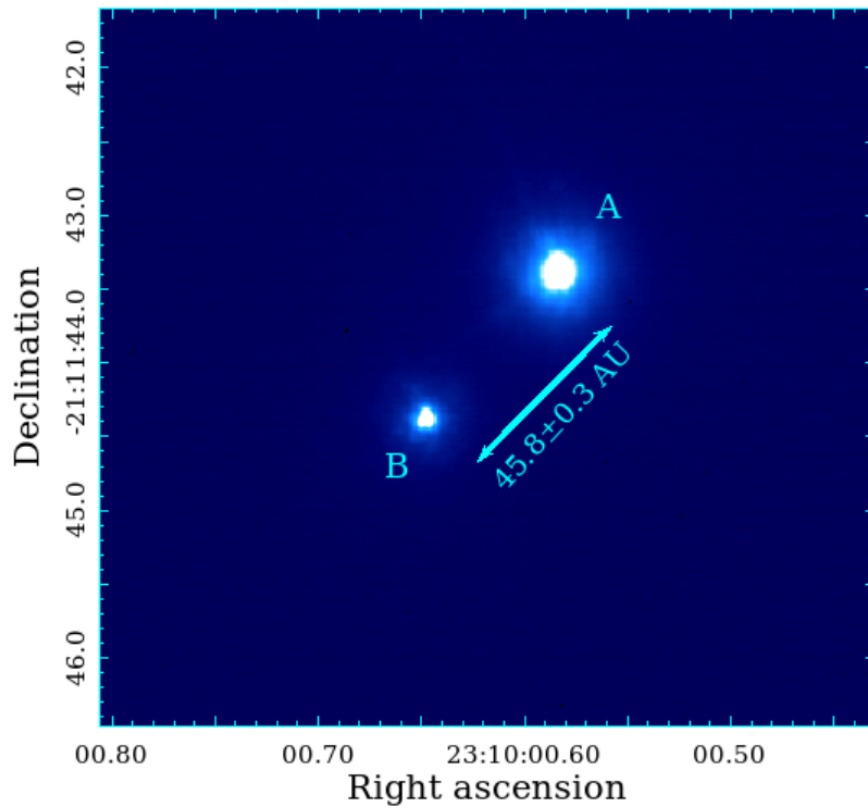

(a) LP 1033-31

(b) LP 877-72

Figure 1: The *J*-band images obtained from VLT/NaCo instruments: (a) LP 1033-31 and (b) LP 877-72. The standard conversion has been used, i.e., north is up, and east is left. A and B denote the primary and secondary components of the VLM binaries.

Table 1: System parameters for LP 1033-31 and LP 877-72

Parameters	LP 1033-31		LP 877-72	
	A	B	A	B
SpT[†]	M4.5±0.5	M4.5±0.5	M1.0±0.3	M3.8±0.3
Mass ($M_\odot$)[††]	0.20±0.04	0.19±0.04	0.520±0.006	0.260±0.005
Radius ($R_\odot$)	0.225±0.030	0.217±0.029	0.492±0.011	0.270±0.006
$T_{\rm eff}$ (K)	3245±107	3211±120	3750±15	3348±10
$\log g$ [‡]	5.061±0.038	5.068±0.039	4.768±0.005	4.984±0.004
Luminosity ($L_\odot$)	0.0050±0.0015	0.0045±0.0014	0.0432±0.0021	0.0082±0.0004

[†] – For the individual systems, the spectral types have been derived from M_J using the method of Scholz et al. (2005); [††] – Mass is derived from the interpolation of Baraffe et al. (2015) isochrones of 5 Gyr; [‡] – $\log g$ is the logarithmic value (base 10) of surface gravity (g), where g is in cm s^{-2} unit.

and secondary components of LP 877-72, the absolute *J*-band magnitudes are derived as 6.44±0.03 and 8.13±0.04, respectively. From the Hertzsprung-Russell Diagram, it is possible to determine the spectral type for each of the components of both systems. Scholz et al. (2005) investigated the relationship between absolute *J* magnitude and the spectral type for K0–L8 stars. From the computed absolute magnitude, we derived the spectral types of the systems LP 1033-31 and LP 877-72 are M4.5+M4.5 and M1+M4, respectively. For comparison, the latest estimated spectral types of the 'unresolved' combined systems of LP 1033-31 and LP 877-72, as derived by Rajpurohit et al. (2013), are given as M4 and M4, respectively. Currently, the spectra of the individual components have not been observed in any of the systems. However, the combined spectra of LP 1033-31 and LP 877-72 have already been observed by Reylé et al. (2006). We also performed a combined spectral fitting using the latest available empirical template library of stellar spectra from Kesseli et al. (2017). We fitted the combined spectra at the flux ratios derived in our analysis. The spectral fitting of the individual components with the derived spectral types is found to be better than the best-fitted template spectra of the unresolved systems. Please also see Karmakar et al. (2020) for a detailed description.

8 Stellar parameters

Stellar magnetic activities are found to be dependent on spectral type as well as stellar age. Investigating 38,000 low-mass stars from the Sloan Digital Sky Survey (SDSS) Data Release 5 (DR5), West et al. (2008) have derived 'activity lifetimes' or ages for each spectral types of M0–M7 dwarfs. As an M4.5+M4.5 binary, the individual components of LP 1033-31 should have an age of 3.5–7.5 Gyr (since the age of M4 and M5 stars are $4.5^{+0.5}_{-1.0}$ and 7.0±0.5 Gyr). On the other hand, the spectral types of LP 877-72 A and B components are M1 and M4, which for a 'single' un-related systems, according to age-activity relations, may have ages <0.8 and $4.5^{+0.5}_{-1.0}$ Gyr, respectively. However, for a physically bound system, it is more likely that both systems are coeval. Further, from the analysis of evolutionary tracks, it has been shown that there are only little significant differences between evolutionary tracks of 0.6–10.0 Gyr (Baraffe et al., 2015). Therefore, we conservatively assume the age of ~5 Gyr. We have estimated the masses of both the components of LP 1033-31 and LP 877-72 using the mass-absolute magnitude relation as derived by Benedict et al. (2016). LP 1033-

31 AB are found to have the nearly equal mass of 0.20±0.04 and 0.19±0.04 $M_\odot$, whereas, for LP 877-72 AB, the derived masses are found to be 0.520±0.006 and 0.260±0.005 $M_\odot$, respectively. Using the mass-radius relations of Boyajian et al. (2012), the radii of LP 1033-31 A and B are derived to be 0.225 ± 0.030 and 0.217 ± 0.029 $R_\odot$. On the other hand, for LP 877-72 AB, the radii are estimated to be 0.492 ± 0.011 and 0.270 ± 0.006 $R_\odot$ for primary and secondary, respectively. Using the measured projected separations and the masses, we estimated the orbital periods for each of the systems from *Kepler*'s law. For LP 1033-31 and LP 877-72, the orbital periods are derived to be 28±3 and 349±3 yrs. For LP 1033-31, the $T_{\rm eff}$ and $\log g$ are found to be similar, whereas the primary of LP 877-72 is derived to be ~400 K hotter and the surface gravity is lower by a factor of ~1.6 than the secondary component. Please see Table 1 for the estimated parameters of detected binary components.

9 Discussion

Using high-resolution adaptive optics NIR JHK_s band images from VLT/NaCo instruments, in this work, we investigated two VLM systems, *viz.* LP 1033-31 and LP 877-72. We found that LP 1033-31 consists of two components with similar brightness, mass, radius, surface temperature, log g, and luminosity. However, in the case of LP 877-72, these parameters vary between the primary and secondary over a wide range. A detailed discussion is beyond the scope of this article. Please find the paper Karmakar et al. (2020) for a robust discussion.

In the remaining part of this section, we will briefly discuss the possibility of hosting exoplanets on the identified VLM components. The radial velocity studies indicate that M-dwarfs host at least $2.39^{+4.58}_{-1.36}$ planets per star orbiting them (Tuomi et al., 2019). Using *Kepler* data, Hardegree-Ullman et al. (2019) estimated the planet occurrence rate for spectral type ranges M3 V – M3.5 V, M4 V – M4.5 V, and M5 V – M5.5 V to be $0.86^{+1.32}_{-0.68}$, $1.36^{+2.30}_{-1.02}$, and $3.07^{+5.49}_{-2.49}$ planets per star. In the case of the binary systems, close binary companions appear to suppress planet formation and hence decrease planet occurrence rates for these systems (see Wang et al., 2014; Kraus et al., 2016). Considering the suppression due to the binarity, we derive that the probability of occurring planet for each of the primary and secondary components of LP 1033-31 AB would be the same and with the range of 4–51%. In the case of LP 877-72, the primary and secondary components of the planet occurrence rate would be ≲ 49%

and 19–208%. In other words, while searching for exoplanets around each of the components of the VLM binaries, we should expect to find up to 'two' exoplanets around LP 877-72 B, in contrast with the LP 877-72 A, LP 1033-31 A, and LP 1033-31 B, all three of the components have the maximum probability of hosting exoplanet are only ~50%.

Acknowledgments

References

Allen P. R., Burgasser A. J., Faherty J. K., Kirkpatrick J. D., 2012, AJ, 144, 62

Apps K., et al., 2010, PASP, 122, 156

Astropy Collaboration et al., 2022, ApJ, 935, 167

Bailer-Jones C. A. L., Rybizki J., Fouesneau M., Mantelet G., Andrae R., 2018, AJ, 156, 58

Baraffe I., Homeier D., Allard F., Chabrier G., 2015, A&A, 577, A42

Baron F., et al., 2015, ApJ, 802, 37

Bate M. R., 2009, MNRAS, 397, 232

Benedict G. F., et al., 2016, AJ, 152, 141

Boyajian T. S., et al., 2012, ApJ, 757, 112

Bradley L., et al., 2022, astropy/photutils: 1.6.0, Zenodo, doi:10.5281/zenodo.7419741

Czesla S., Schröter S., Schneider C. P., Huber K. F., Pfeifer F., Andreasen D. T., Zechmeister M., 2019, PyA: Python astronomy-related packages, Astrophysics Source Code Library, record ascl:1906.010 (ascl:1906.010)

Delfosse X., Forveille T., Ségransan D., Beuzit J.-L., Udry S., Perrier C., Mayor M., 2000, A&A, 364, 217

Dittmann J. A., Irwin J. M., Charbonneau D., Newton E. R., 2016, ApJ, 818, 153

Dupuy T. J., Liu M. C., 2017, ApJS, 231, 15

Finch C. T., Zacharias N., Subasavage J. P., Henry T. J., Riedel A. R., 2014, AJ, 148, 119

Frith J., et al., 2013, MNRAS, 435, 2161

Gaia Collaboration et al., 2018, A&A, 616, A1

Gálvez-Ortiz M. C., Solano E., Lodieu N., Aberasturi M., 2017, MNRAS, 466, 2983

Giclas H. L., Burnham R. J., Thomas N. G., 1978, Lowell Observatory Bulletin, 8, 89

Hardegree-Ullman K. K., Cushing M. C., Muirhead P. S., Christiansen J. L., 2019, AJ, 158, 75

Hartung M., Bizenberger P., Boehm A., Laun W., Lenzen R., Wagner K., 2000, in Iye M., Moorwood A. F., eds, Society of Photo-Optical Instrumentation Engineers (SPIE) Conference Series Vol. 4008, Optical and IR Telescope Instrumentation and Detectors. pp 830–841, doi:10.1117/12.395543

Hartung M., Blanc A., Fusco T., Lacombe F., Mugnier L. M., Rousset G., Lenzen R., 2003, A&A, 399, 385

Karmakar S., 2019, PhD thesis, ARIES, Nainital, India; PRSU, Raipur, India, doi:10.5281/zenodo.5762548

Karmakar S., 2021, MIRA Newsletter, 44, 3

Karmakar S., Pandey J. C., 2018, Bulletin de la Societe Royale des Sciences de Liege, 87, 163

Karmakar S., et al., 2016, MNRAS, 459, 3112

Karmakar S., Pandey J. C., Airapetian V. S., Misra K., 2017, ApJ, 840, 102

Karmakar S., Pandey J. C., Naik S., Savanov I. S., Raj A., 2019, Bulletin de la Societe Royale des Sciences de Liege, 88, 182

Karmakar S., Rajpurohit A. S., Allard F., Homeier D., 2020, MNRAS, 498, 737

Karmakar S., Naik S., Pandey J. C., Savanov I. S., 2022, MNRAS, 509, 3247

Karmakar S., Naik S., Pandey J. C., Savanov I. S., 2023, MNRAS, 518, 900

Kesseli A. Y., West A. A., Veyette M., Harrison B., Feldman D., Bochanski J. J., 2017, ApJS, 230, 16

Kirkpatrick J. D., et al., 2016, ApJS, 224, 36

Kraus A. L., Ireland M. J., Huber D., Mann A. W., Dupuy T. J., 2016, AJ, 152, 8

Lenzen R., Hofmann R., Bizenberger P., Tusche A., 1998, in Fowler A. M., ed., Society of Photo-Optical Instrumentation Engineers (SPIE) Conference Series Vol. 3354, Infrared Astronomical Instrumentation. pp 606–614, doi:10.1117/12.317287

Lépine S., Gaidos E., 2011, AJ, 142, 138

Luyten W. J., 1995, VizieR Online Data Catalog, p. I/98A

Muirhead P. S., Dressing C. D., Mann A. W., Rojas-Ayala B., Lépine S., Paegert M., De Lee N., Oelkers R., 2018, AJ, 155, 180

Pandey J. C., Karmakar S., 2015, AJ, 149, 47

Patel M. K., Pandey J. C., Karmakar S., Srivastava D. C., Savanov I. S., 2016, MNRAS, 457, 3178

Phan-Bao N., Martín E. L., Reylé C., Forveille T., Lim J., 2005, A&A, 439, L19

Pokorny R. S., Jones H. R. A., Hambly N. C., 2003, A&A, 397, 575

Rajpurohit A. S., Reylé C., Allard F., Homeier D., Schultheis M., Bessell M. S., Robin A. C., 2013, A&A, 556, A15

Reiners A., et al., 2018, A&A, 612, A49

Reylé C., Robin A. C., 2004, A&A, 421, 643

Reylé C., Scholz R.-D., Schultheis M., Robin A. C., Irwin M., 2006, MNRAS, 373, 705

Rousset G., et al., 1998, in Bonaccini D., Tyson R. K., eds, Society of Photo-Optical Instrumentation Engineers (SPIE) Conference Series Vol. 3353, Adaptive Optical System Technologies. pp 508–516, doi:10.1117/12.321686

Rousset G., et al., 2000, in Wizinowich P. L., ed., Society of Photo-Optical Instrumentation Engineers (SPIE) Conference Series Vol. 4007, Adaptive Optical Systems Technology. pp 72–81, doi:10.1117/12.390304

Salim S., Gould A., 2003, ApJ, 582, 1011

Savanov I. S., et al., 2016, AcA, 66, 381

Savanov I. S., Dmitrienko E. S., Karmakar S., Pandey J. C., 2018, Astronomy Reports, 62, 532

Savanov I. S., Naroenkov S. A., Nalivkin M. A., Pandey J. C., Karmakar S., 2019, Astronomy Letters, 45, 602

Schneider A. C., Greco J., Cushing M. C., Kirkpatrick J. D., Mainzer A., Gelino C. R., Fajardo-Acosta S. B., Bauer J., 2016, ApJ, 817, 112

Scholz R.-D., Meusinger H., Jahreiß H., 2005, A&A, 442, 211

Skrutskie M. F., et al., 2006, AJ, 131, 1163

Spanoudakis P., Zago L., Chetelat O., Gentsch R., Mato Mira F., 2000, in Wizinowich P. L., ed., Society of Photo-Optical Instrumentation Engineers (SPIE) Conference Series Vol. 4007, Adaptive Optical Systems Technology. pp 408–415, doi:10.1117/12.390352

Stassun K. G., et al., 2019, AJ, 158, 138

Tody D., 1986, The IRAF Data Reduction and Analysis System. p. 733, doi:10.1117/12.968154

Tody D., 1993, IRAF in the Nineties. p. 173

Tuomi M., et al., 2019, arXiv e-prints, p. arXiv:1906.04644

Wang J., Fischer D. A., Xie J.-W., Ciardi D. R., 2014, ApJ, 791, 111

West A. A., Hawley S. L., Bochanski J. J., Covey K. R., Reid I. N., Dhital S., Hilton E. J., Masuda M., 2008, AJ, 135, 785

Winters J. G., et al., 2015, AJ, 149, 5

Winters J. G., et al., 2019, AJ, 157, 216

Wright E. L., et al., 2010, AJ, 140, 1868

Wroblewski H., Torres C., 1995, A&AS, 110, 27

York D. G., et al., 2000, AJ, 120, 1579